energies

MDPI

Article

Impacts of Heat-Conducting Solid Wall and Heat-Generating Element on Free Convection of Al_2O_3/H_2O Nanofluid in a Cavity with Open Border

Mikhail A. Sheremet [1,*], Hakan F. Oztop [2], Dmitriy V. Gvozdyakov [3] and Mohamed E. Ali [4]

1 Laboratory on Convective Heat and Mass Transfer, Tomsk State University, 634050 Tomsk, Russia
2 Department of Mechanical Engineering, Technology Faculty, Firat University, 23119 Elazig, Turkey; hfoztop1@gmail.com
3 The Butakov Research Center, Tomsk Polytechnic University, 634050 Tomsk, Russia; dim2003@tpu.ru
4 Department of Mechanical Engineering, College of Engineering, King Saud University, 11421 Riyadh, Saudi Arabia; mali@ksu.edu.sa
* Correspondence: sheremet@math.tsu.ru; Tel.: +7-3822-529740

Received: 7 November 2018; Accepted: 5 December 2018; Published: 7 December 2018

Abstract: Development of modern electronic devices demands a creation of effective cooling systems in the form of active or passive nature. More optimal technique for an origination of such cooling arrangement is a mathematical simulation taking into account the major physical processes which define the considered phenomena. Thermogravitational convection in a partially open alumina-water nanoliquid region under the impacts of constant heat generation element and heat-conducting solid wall is analyzed numerically. A solid heat-conducting wall is a left vertical wall cooled from outside, while a local solid element is placed on the base and kept at constant volumetric heat generation. The right border is supposed to be partially open in order to cool the local heater. The considered domain of interest is an electronic cabinet, while the heat-generating element is an electronic chip. Partial differential equations of mathematical physics formulated in non-primitive variables are worked out by the second order finite difference method. Influences of the Rayleigh number, heat-transfer capacity ratio, location of the local heater and nanoparticles volume fraction on liquid circulation and thermal transmission are investigated. It was ascertained that an inclusion of nanosized alumina particles to the base liquid can lead to the average heater temperature decreasing, that depends on the heater location and internal volumetric heat generation. Therefore, an inclusion of nanoparticles inside the host liquid can essentially intensify the heat removal from the heater that is the major challenge in different engineering applications. Moreover, an effect of nanosized alumina particles is more essential in the case of low intensive convective flow and when the heater is placed near the cooling wall.

Keywords: thermogravitational convection; nanofluid; local heat-generating element; heat-conducting solid wall; partially open cavity; finite difference technique

1. Introduction

Convective thermal transmission in partially open cavities with solid heat-conducting walls and heat-generating elements is very important in different engineering supplements, e.g., cooling of electronics, heat-transfer devices, chemical apparatus and solar collectors. It should be noted that nowadays one of the major challenges is a creation of effective cooling system for reducing the working temperature for heat-generating elements inside different electronic cabinets. Optimal approach for solution to this problem is an employment of computer power of modern computational systems

combined with numerical methods of hydrodynamics and heat transfer. Different interesting and useful theoretical and experimental data have been announced during last decades.

Thus, Dwesh K. Singh and S.N. Singh [1] examined numerically 2D conjugate free convection-radiation heat transfer in an open air domain under the influence of uniform volumetric heat generating element on the vertical border. They used Hottel's Crossed-string technique for calculation of view factors during the surface radiation analysis. Taking into account the obtained results, correlations were derived for maximum dimensionless heater temperature for various positions. Mikhailenko et al. [2] conducted a computational analysis of convective heat transfer and thermal radiation inside a rotating cavity with a heat-generating element. They showed that domain rotating velocity and surface emissivity of surrounding walls and heated source are very effective control parameters for creation of optimal cooling system. Chen et al. [3] evaluated the convection-conduction thermal transmission in an open partially porous domain. They chose the lattice Boltzmann approach to solve equations. Naylor et al. [4] studied numerically thermogravitational convection from a window glazing with an insect shield simulated like a porous layer and found that the shield has negligible influence on convective thermal transmission for high values of *Ra*. Astanina et al. [5] analyzed numerically thermogravitational convection in a partially porous cavity with a heat-generating source. The authors demonstrated that porous layer thickness and variable viscosity parameter of the working medium allows optimizing the passive cooling arrangement owing to an enhancement of cooling impact from the cold vertical borders. Rahman et al. [6] examined the influence of Ohmic heating and magnetic field on mixed convection heat and mass transfer in a horizontal channel using finite element technique.Their results demonstrated that the aforesaid fields affect the flow structure, thermal and mass transmnission. Saha et al. [7] worked on MHD mixed convection under the influence of internal heat generation/absorption. They revealed that the average Nusselt number is a decreasing function of the heat generation and an increasing function of heat absorption. Gangawane [8] made a numerical study on MHD thermograviational convection in an open cavity. The author found that the domain of interest with the inclined magnetic field at the angle $\pi/4$ illustrates the highest thermal transmission restriction than other analyzed conditions. Dong and Li [9] studied the conjugate free convection in a composite closed space by vorticity–stream function technique. They found that used material, geometry and *Ra* are efffective parameters for an optimization of thermal transmission. Bilgen [10] performed a work on free convection in closed spaces having thin obstacle on heated border. He observed that length and location of this obstacle are very good control elements for an intensification of liquid circulation and thermal transmission.

Nowadays, for an intensification of heat transfer within different engineering systmes the nanosized metal or metal oxide particles are used [11–13]. Different experimental studies showed that an inclusion of nanoparticles of low concentration can improve the heat transfer performance inside the system [14,15]. Thus, Asirvatham et al. [14] performed experiments for steady convection thermal transmission of de-ionized water combined with copper oxide nanoparticles of low concentration (0.003% by volume) in a copper tube. They showed 8% enhancement of the convective heat transfer coefficient of the nanofluid even with a low volume concentration of nanosized copper oxide particles. Raei et al. [15] experimentally studied the circulation and thermal transmission parameters of three kinds of the nanofluids within a fin-and-tube heat exchanger. It was revealed that an inclusion of alumina nanosized particles into the water enhances the overall heat transfer parameter and friction factor up to 20% and 5%, respectively. Taking into account such heat transfer enhancement, these approach can be used for an intesification of cooling process inside the electronic cabinets. Several theoretical and experimental works were published. Thus, Mehrez et al. [16] solved numerically a problem on mixed convection combined with entropy production with an open region filled with nanoliquid under the bottom heating impact. They found that the thermal transmission combined with entropy production are enhanced with the growth of *Re*, *Ri* and nanoparticles concentration, and changed with region *AR* and nanoparticle types. Sheremet et al. [17] analyzed mixed convective heat and mass transport inside a porous nanoliquid domain with open border under the impacts

of thermophoresis and Brownian diffusion. They revealed that the average Nusselt parameter is a growing mapping of *Ra* and *Re* and a reduced mapping of *Le*. Sheremet et al. [18] investigated nanoliquid free convection within a semi-open tall wavy cavity under the effects of horizontal temperature difference and Buongiorno's nanofluid model. They ascertained that a growth of the shape coefficient (<1.0) results in the thermal transmission intensification, while a rise of this parameter in a range of (>1.0) results in non-monotonic behavior for the average dimensionless heat transfer coefficient owing to significant heating of the wave trough. Bondareva et al. [19] examined MHD nanofluid free convective thermal transmission in a tilted wavy tall porous domain with a local heater using streamlines and heatlines. Optimal parameters for the thermal transmission intensification were found. Miroshnichenko et al. [20] studied computationally natural convective heat transfer of Al_2O_3/H_2O nanoliquid in an inclined open chamber with a heat-generating source. They illustrated that the major cooling of the heater occurs for central element position with chamber inclination angle of $\pi/3$. Bondarenko et al. [21] performed a numerical work on free convection of alumina/water nanoliquid in an enclosure with heat-generating solid source. It was ascertained that within hermetic electronic cabinet having a heat-generating source under cold vertical isothermal borders the thermal removal from the heater can be enhanced by including nanosized aluminum oxide particles of small volume fraction (1%) and by the position of the heated element near the cold vertical border.

The abovementioned brief review shows that the problem of heat transfer enhancement within electronic cabinets is very important and usage of nanoparticles with additional steps can help to solve such challenge. Therefore, the aim of this work is to calculate free convection thermal transmission in a partially open alumina-water nanoliquid area under the effect of vertical solid mural and local heat-generating source. The present study is devoted to development of passive cooling arrangement for heat-generating elements using the nanoliquids under the impacts of heat-conducting walls and local opening ports. The present study is a continuation of passive cooling systems analysis that was presented in the case of open inclined cavity [20] and closed vertical chamber [21]. Novelty of the present investigation is an examination of free convection under the combined impacts of open border, cooled solid wall of finite thickness and heat-generating element.

2. Basic Equations

The considered region with frame of reference and boundary conditions is demonstrated in Figure 1. It is a vertical cavity having isothermally cooling left vertical wall, while this solid wall has finite thickness l and finite thermal conductivity k_w. Horizontal walls of neglecting thickness are adiabatic. Right vertical wall is adiabatic also but it has an open port of size d where ambient cold nanofluid can penetrate into the cavity and it also can exit from the cavity. Solid heater is placed at the base of the cavity and it has a permanent volumetric heat flux Q. Length from the left border to this heated element is s. The nanoliquid is a solution of water with solid spherical alumina nanosized particles [20–22].

The partial differential equations of mathematical physics for 2D free convection nanoliquid circulation and thermal transmission within the considered domain (see Figure 1) employing the conservation laws are written:

- for the nanoliquid

$$\frac{\partial \overline{u}}{\partial \overline{x}} + \frac{\partial \overline{v}}{\partial \overline{y}} = 0 \tag{1}$$

$$\rho_{nf}\left(\frac{\partial \overline{u}}{\partial t} + \overline{u}\frac{\partial \overline{u}}{\partial \overline{x}} + \overline{v}\frac{\partial \overline{u}}{\partial \overline{y}}\right) = -\frac{\partial p}{\partial \overline{x}} + \mu_{nf}\left(\frac{\partial^2 \overline{u}}{\partial \overline{x}^2} + \frac{\partial^2 \overline{u}}{\partial \overline{y}^2}\right) \tag{2}$$

$$\rho_{nf}\left(\frac{\partial \overline{v}}{\partial t} + \overline{u}\frac{\partial \overline{v}}{\partial \overline{x}} + \overline{v}\frac{\partial \overline{v}}{\partial \overline{y}}\right) = -\frac{\partial p}{\partial \overline{y}} + \mu_{nf}\left(\frac{\partial^2 \overline{v}}{\partial \overline{x}^2} + \frac{\partial^2 \overline{v}}{\partial \overline{y}^2}\right) + (\rho\beta)_{nf} g (T - T_c) \tag{3}$$

$$\frac{\partial T}{\partial t} + \overline{u}\frac{\partial T}{\partial \overline{x}} + \overline{v}\frac{\partial T}{\partial \overline{y}} = \frac{k_{nf}}{(\rho c)_{nf}}\left(\frac{\partial^2 T}{\partial \overline{x}^2} + \frac{\partial^2 T}{\partial \overline{y}^2}\right) \tag{4}$$

- for the heater

$$(\rho c)_{hs}\frac{\partial T}{\partial t} = k_{hs}\left(\frac{\partial^2 T}{\partial \overline{x}^2} + \frac{\partial^2 T}{\partial \overline{y}^2}\right) + Q \tag{5}$$

- for the solid wall

$$(\rho c)_{w}\frac{\partial T}{\partial t} = k_{w}\left(\frac{\partial^2 T}{\partial \overline{x}^2} + \frac{\partial^2 T}{\partial \overline{y}^2}\right) \tag{6}$$

The considered nanoliquid viscosity and heat-transfer capacity are the mappings of nanosized particles concentration as obtained by Ho et al. [22].

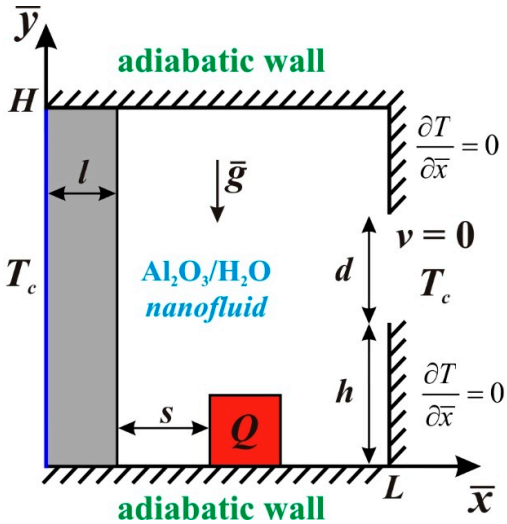

Figure 1. Analyzed region and reference frame.

Including the stream function $\left(\overline{u} = \frac{\partial \overline{\psi}}{\partial \overline{y}}, \overline{v} = -\frac{\partial \overline{\psi}}{\partial \overline{x}}\right)$, vorticity $\left(\overline{\omega} = \frac{\partial \overline{v}}{\partial \overline{x}} - \frac{\partial \overline{u}}{\partial \overline{y}}\right)$, and the non-dimensional parameters:

$$x = \overline{x}/L,\ y = \overline{y}/L,\ \tau = t\sqrt{g\beta\Delta T/L},\ \theta = (T - T_c)/\Delta T,$$
$$u = \overline{u}/\sqrt{g\beta\Delta TL},\ v = \overline{v}/\sqrt{g\beta\Delta TL},\ \psi = \overline{\psi}/\sqrt{g\beta\Delta TL^3},\ \omega = \overline{\omega}\sqrt{L/g\beta\Delta T}$$

the control equations of mathematical physics become:

- for the nanofluid

$$\frac{\partial^2 \psi}{\partial x^2} + \frac{\partial^2 \psi}{\partial y^2} = -\omega \tag{7}$$

$$\frac{\partial \omega}{\partial \tau} + u\frac{\partial \omega}{\partial x} + v\frac{\partial \omega}{\partial y} = H_1(\phi)\sqrt{\frac{Pr}{Ra}}\left(\frac{\partial^2 \omega}{\partial x^2} + \frac{\partial^2 \omega}{\partial y^2}\right) + H_2(\phi)\frac{\partial \theta}{\partial x} \tag{8}$$

$$\frac{\partial \theta}{\partial \tau} + u\frac{\partial \theta}{\partial x} + v\frac{\partial \theta}{\partial y} = \frac{H_3(\phi)}{\sqrt{Ra \cdot Pr}}\left(\frac{\partial^2 \theta}{\partial x^2} + \frac{\partial^2 \theta}{\partial y^2}\right) \tag{9}$$

- for the heater

$$\frac{\partial \theta}{\partial \tau} = \frac{\alpha_{hs}/\alpha_f}{\sqrt{Ra \cdot Pr}}\left(\frac{\partial^2 \theta}{\partial x^2} + \frac{\partial^2 \theta}{\partial y^2} + 1\right) \tag{10}$$

- for the solid wall

$$\frac{\partial\theta}{\partial\tau} = \frac{\alpha_w/\alpha_f}{\sqrt{Ra\cdot Pr}}\left(\frac{\partial^2\theta}{\partial x^2}+\frac{\partial^2\theta}{\partial y^2}\right) \tag{11}$$

The considered additional conditions are

$$\begin{aligned}
&\tau = 0: \quad \psi = \omega = \theta = 0 \text{ at } 0 \le x \le 1 \text{ and } 0 \le y \le A = H/L \\
&\tau > 0: \quad \theta = 0 \text{ at } x = 0 \text{ and } 0 \le y \le A \\
&\qquad \psi = 0,\ \omega = -\frac{\partial^2\psi}{\partial y^2},\ \frac{\partial\theta}{\partial y} = 0 \text{ at } y = 0,\ A \text{ and } 0 < x < 1 \\
&\qquad \psi = 0,\ \omega = -\frac{\partial^2\psi}{\partial x^2},\ \frac{\partial\theta}{\partial x} = 0 \text{ at } x = 1 \text{ and } 0 < y \le \zeta = h/L \\
&\qquad \psi = 0,\ \omega = -\frac{\partial^2\psi}{\partial x^2},\ \frac{\partial\theta}{\partial x} = 0 \text{ at } x = 1 \text{ and } h/L + d/L = \zeta + \eta \le y < A
\end{aligned} \tag{12}$$

$$\begin{aligned}
&\tau > 0: \quad \frac{\partial\psi}{\partial x} = 0, \quad \frac{\partial\omega}{\partial x} = 0, \quad \begin{cases} \text{if } \frac{\partial\psi}{\partial y} \ge 0 \text{ then } \frac{\partial\theta}{\partial x} = 0 \\ \text{if } \frac{\partial\psi}{\partial y} < 0 \text{ then } \theta = 0 \end{cases} \text{ at } x = 1 \text{ and } \zeta < y < \zeta + \eta \\
&\qquad \psi = 0,\ \omega = -\frac{\partial^2\psi}{\partial n^2},\ \begin{cases} \theta_{hs} = \theta_{nf} \\ \frac{\partial\theta_{hs}}{\partial n} = H_4(\phi)\frac{\partial\theta_{nf}}{\partial n} \end{cases} \text{ at heat source surface} \\
&\qquad \psi = 0,\ \omega = -\frac{\partial^2\psi}{\partial x^2},\ \begin{cases} \theta_w = \theta_{nf} \\ \frac{\partial\theta_w}{\partial x} = H_5(\phi)\frac{\partial\theta_{nf}}{\partial x} \end{cases} \text{ at } x = \xi = l/L \text{ and } 0 \le y \le A
\end{aligned} \tag{13}$$

Here additional parameters are

$$\begin{aligned}
&Ra = \frac{\rho g\beta\Delta TL^3}{\alpha\mu}, \quad Pr = \frac{\mu}{\rho\alpha}, \quad \Delta T = \frac{QL^2}{k_{hs}}, \quad H_1(\phi) = \frac{1+4.93\phi+222.4\phi^2}{1-\phi+\phi\rho_p/\rho_f}, \\
&H_2(\phi) = \frac{1-\phi+\phi(\rho\beta)_p/(\rho\beta)_f}{1-\phi+\phi\rho_p/\rho_f}, \quad H_3(\phi) = \frac{1+2.944\phi+19.672\phi^2}{1-\phi+\phi(\rho c)_p/(\rho c)_f}, \\
&H_4(\phi) = \frac{1+2.944\phi+19.672\phi^2}{k_{hs}/k_f}, \quad H_5(\phi) = \frac{1+2.944\phi+19.672\phi^2}{k_w/k_f}
\end{aligned} \tag{14}$$

The heat transfer rate can be described by the average Nusselt number at the heater surface:

$$\overline{Nu} = \frac{1}{\gamma}\int_0^\gamma \left(-\frac{k_{nf}}{k_f}\frac{\partial\theta}{\partial n}\right)d\gamma \tag{15}$$

3. Numerical Technique

The governing Equations (7)–(11) with additional conditions (12) and (13) were resolved by the finite difference technique using the uniform grid. The detailed verification of the developed computational code was conduced earlier in refs. [17–21].

In the case of nanoliquid free convection inside the differentially heated square chamber, the obtained data were compared with experimental results of Ho et al. [22] and numerical results of Saghir et al. [23]. Table 1 shows a very good agreement between the considered data.

Table 1. Mean *Nu* at heated border compared with results of other authors.

Dimensionless Parameters	φ	Obtained Data	Results of Ho et al. [22]	Results of Saghir et al. [23]
$Ra = 8.663 \times 10^7$, $Pr = 7.002$	0.01	31.6043	32.2037	30.657
	0.02	31.2538	31.0905	30.503
	0.03	30.829	29.0769	30.205

In the case of free convection inside the partially open chamber, the developed computational code was validated successfully using the numerical data of Mohamad et al. [24] and Kefayati [25] (see Table 2).

Table 2. Mean Nu at heated border compared with results of other authors.

Ra	Obtained Data	Results of Mohamad et al. [24]	Results of Kefayati [25]
10^4	3.321	3.377	3.319
10^5	7.325	7.323	7.391
10^5	14.322	14.380	14.404

The solution technique was tested using various uniform grids. Figure 2 demonstrates the impact of the considered meshes on $\overline{Nu}$, average heater temperature and nanofluid flow intensity for $Ra = 10^5$, $Pr = 6.82$, $K_r = k_w/k_f = 10$, $\varphi = 0.02$, $\delta = s/L = 0.3$, $h/L = 0.2$, $l/L = 0.1$ and $d/L = 0.5$.

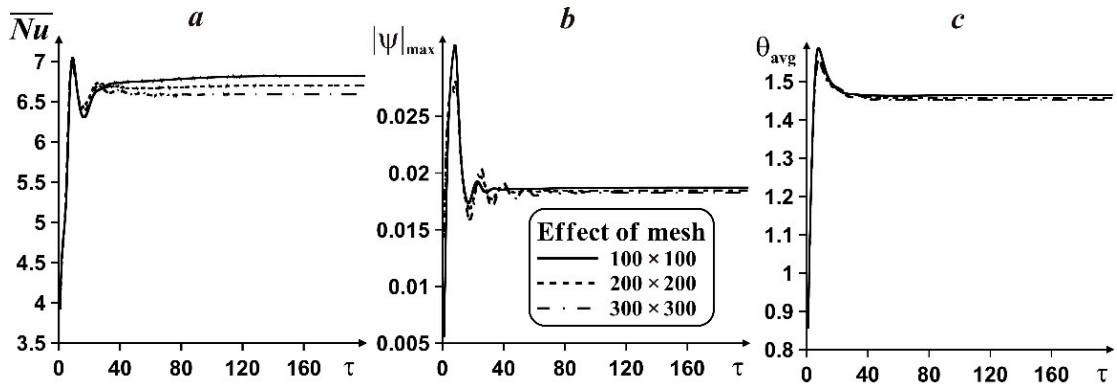

Figure 2. Behavior of the average Nusselt number (**a**), nanoliquid flow rate (**b**) and average heater temperature (**c**) with the non-dimensional time and grid characteristics.

The presented data in Figure 2 shows that differences between the considered uniform grids of 200 × 200 nodes and 300 × 300 nodes are non-essential. Therefore, taking into account the calculation accuracy and the computational time, the mesh of 200 × 200 nodes was chosen for the base investigation.

4. Results

This paragraph deals with computational study of the nanoliquid circulation and heat transfer within the considered domain under the influence of the following characteristics: Rayleigh number ($10^3 \leq Ra \leq 10^5$), Prandtl number ($Pr = 6.82$), thermal conductivity ratio ($1 \leq K_r = k_w/k_f \leq 20$), heater location ($0.1 \leq \delta = s/L \leq 0.5$) and nanoparticles volume fraction ($0 \leq \varphi \leq 0.04$) for $h/L = 0.2$, $l/L = 0.1$ and $d/L = 0.5$. The analysis pays attention in the description of Ra, K_r, heater location and nanoparticles concentration impacts. Isolines of stream function and temperature, $\overline{Nu}$, nanoliquid circulation rate and mean heater temperature for various control characteristics are pictured in Figures 3–12. It is worth noting that such investigation can help to understand the nanoliquid behavior and heat transfer performance within the considered partially open cavity with the heat-conducting solid wall and heat-generating silicon element.

Figure 3 presents isolines of stream function and temperature within the considered region for $K_r = 5$, $\delta = 0.2$ and various Ra. For the present study an increase in Ra is related to a raise of the internal heater generation Q.

In the case of low and moderate Ra (10^3 and 10^4) one convective cell is formed near the internal surface of the heat-conducting solid wall and another one characterizes an intrusion of cold nanoliquid from the open port inside the region. An appearance of the convective cell near the solid wall is explained by the formation of temperature difference between the cold solid border and hot heat-generating element. Therefore, this circulation reflects a counter-clockwise motion of nanofluid. Moreover, the penetrative flow from the open border begins to interact with the abovementioned vortex and the line of such interaction corresponds to the thermal plume appeared above the heat

source. A growth of the internal heat generation leads to a deformation of the vortex near the solid wall due to more intensive penetrative flow. For $Ra = 10^5$ (Figure 3c) this convective cell is divided into two recirculations located in top and lower parts of the solid wall. Isotherms reflect a distribution of temperature within the region and solid wall. Heating occurs from the element located on the bottom wall, while cooling occurs from outside near the left solid border and from the open part of the right boundary. For $Ra = 10^3$ (Figure 3a) the dominated thermal transmission mode is a thermal conduction and as a result the isotherms are parallel to the heated and cooled elements. Moreover, more essential cooling occurs in the upper part of the left vertical wall due to less intensive heating from the heater. It is interesting to note that the heat-generating element is a solid block and heat conduction Equation (10) is solved within this element, but isotherms are not presented inside the heater. The main reason for such behavior is the high value of silicon thermal conductivity as the heater material in comparison with the thermal conductivity of working medium. As a result, this element is heated quickly.

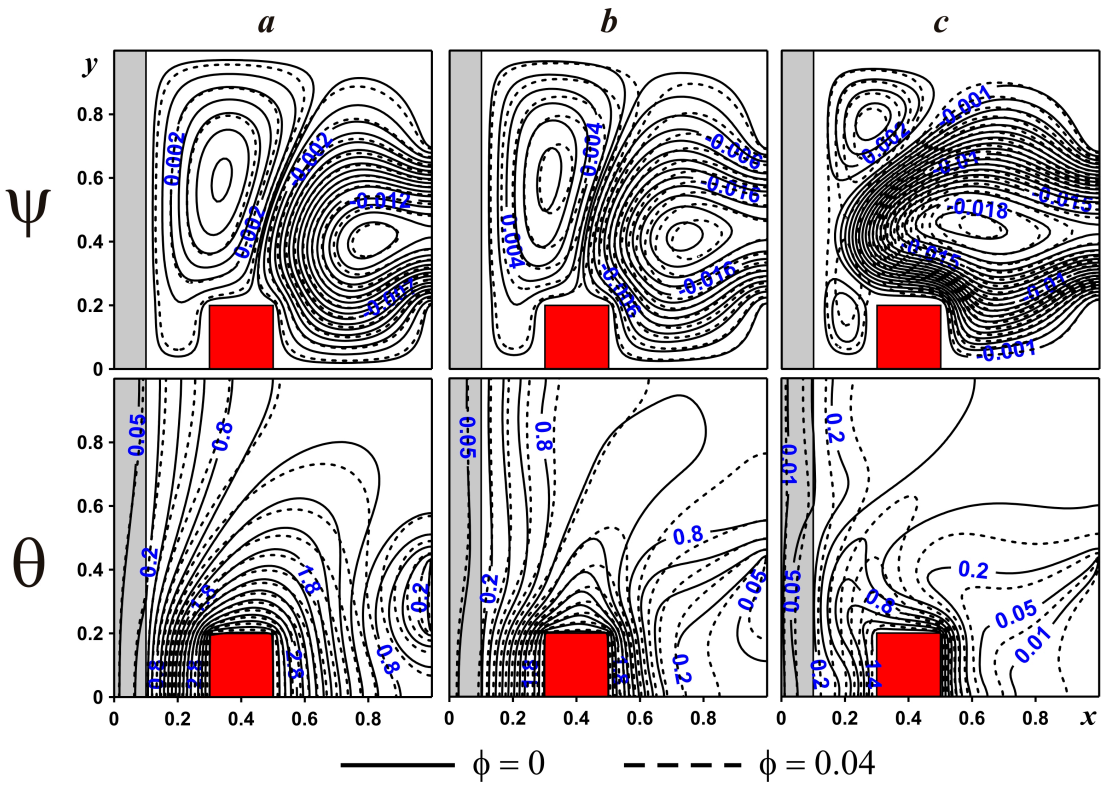

Figure 3. Streamlines ψ and isotherms θ for $K_r = 5$, $\delta = 0.2$: $Ra = 10^3$ (**a**), $Ra = 10^4$ (**b**), $Ra = 10^5$ (**c**).

An increment in the temperature difference ($Ra = 10^4$ in Figure 3b) leads to more essential cooling from the cold parts and heating from the element with intensification of convective thermal transmission in the central part of the domain. It is worth noting here that thermal plume is more essential with pronounced plume's shape. Due to the prevalence of thermal conduction in a spacing between the solid border and heated element, heating of the solid wall occurs in the bottom part from the heater. While for high value of Ra (10^5 in Figure 3c) heating of the solid wall from the heater occurs in the bottom part but over the wall from the tilted thermal plume due to the convective thermal transmission intensification. A growth of Ra results also in more essential cooling from the open port. It is worth noting, that distortion of thermal plume for $Ra = 10^5$ occurs owing to the significant impact of penetrative nanoliquid on convective flow over the heater.

An inclusion of alumina nanosized particles to the clear water results in the small changes for the thermal conduction dominated mode ($Ra = 10^3$ in Figure 3a), while for convective heat transfer,

cooling of the cavity occurs essentially owing to high magnitude of the effective heat-transfer capacity (see ref. [22]).

Impacts of Ra and φ on the mean parameters are shown in Figure 4. The presented parameters have been normalized using the temperature difference that depends on the volumetric heat generation. Therefore, for comparison between different Rayleigh numbers it is necessary to normalize using the general scale. An increase in the temperature difference results in an essential rise of $\overline{Nu}$ owing to more intensive circulation of the working liquid. While a raise of φ results in a diminution of $\overline{Nu}$. The nanoliquid circulation rate $|\psi|_{max}\sqrt{Ra \cdot Pr}$ increases with Ra, due to more intensive circulation for high ΔT. An increment of nanoparticles volume fraction reduces $|\psi|_{max}$ also due to a rise of the nanofluid viscosity. A growth of ΔT reflects a rise of θ_{avg} using the normalization with general scale. An enhancement of φ allows decreasing the average temperature for heat conduction regime ($Ra = 10^3$), while for the transition heat transfer ($Ra = 10^4$) and heat convection ($Ra = 10^5$) θ_{avg} increases with the nanoparticles concentration.

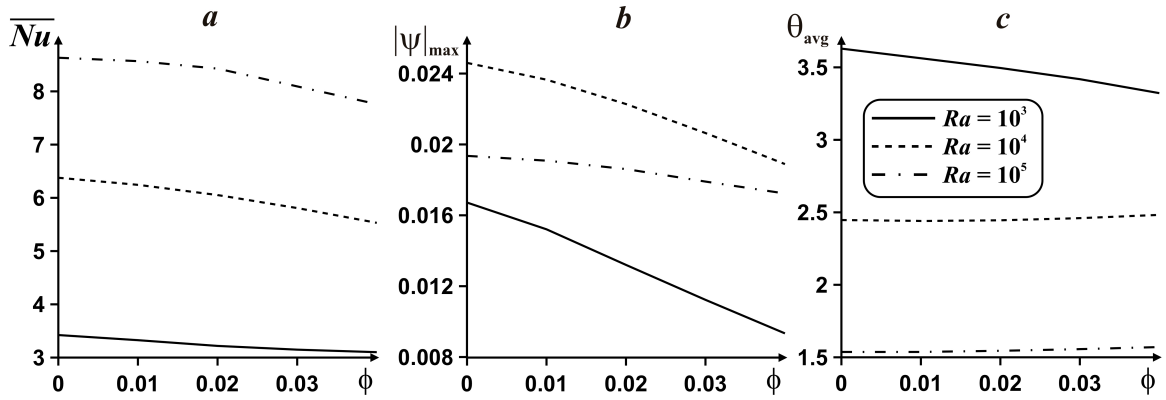

Figure 4. Dependences of the average Nusselt number (**a**), nanoliquid circulation rate (**b**) and mean heater temperature (**c**) on φ and Ra for $K_r = 5$, $\delta = 0.2$.

Figure 5 indicates the impacts of K_r between solid border material and host fluid on isolines of stream function and temperature for $Ra = 10^5$, $\delta = 0.2$. Regardless of the thermal conductivity ratio values, two recirculations are appeared close to the solid boundary in the upper and bottom parts, while major circulation appears from the open port. An enhancement of the solid border heat-transfer capacity results in an intensification of recirculations near the solid wall due to more intensive cooling of this wall, where cold temperature is transported intensively from the external surface till internal one and temperature gradient at this internal surface increases. The latter characterizes an intensification of convective flow near this wall that can deform the nanofluid penetration flow from the open border. Essential cooling of the heat-conducting solid wall can be found in Figure 5 with distributions of isotherms. An increment of isothermal lines density close to the solid-fluid interface ($x = 0.1$) illustrates an origin of strong temperature gradient at this wall. More significant temperature differences are found along the right and top surfaces of the local heater owing to a reciprocal action between hot and cold temperature waves. Addition of nanoparticles reflects a formation of more stable circulation close to the left solid border, where for $K_r \geq 5$ one can find alone convective cell, while for $\varphi = 0$ we have two different circulations in upper and bottom parts. As a result, it is possible to conclude that a growth of thermal conductivity ratio related with an increment of solid wall thermal conductivity leads to an intensification of convective recirculation near the upper part of the internal surface of this heat-conducting wall owing to high cooling rate from the border $x = 0$.

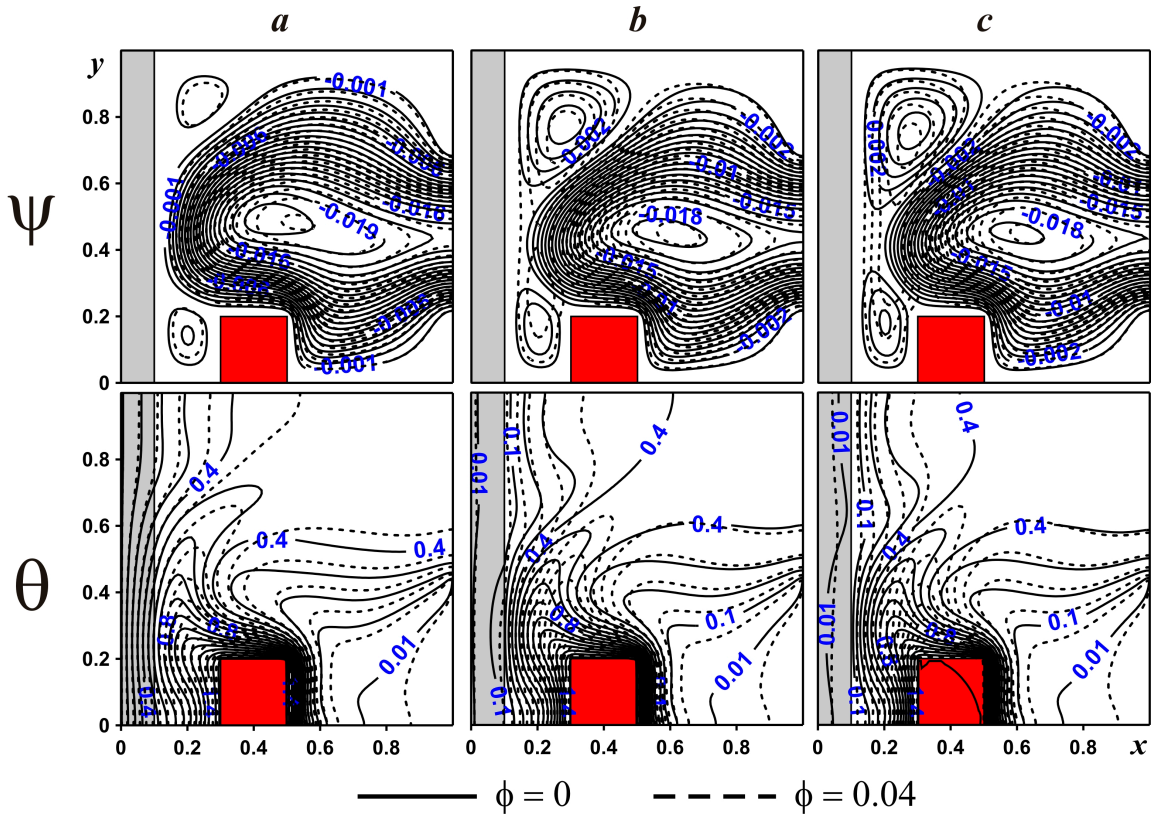

Figure 5. Streamlines ψ and isotherms θ for $Ra = 10^5$, $\delta = 0.2$: $K_r = 1$ (**a**), $K_r = 5$ (**b**), $K_r = 20$ (**c**).

Figures 6–8 present the effects of K_r, φ and Ra on the integral parameters such as $\overline{Nu}$, $|\psi|_{max}$ and θ_{avg} for $\delta = 0.2$. As can be found from this figure, impacts of Ra and nanoparticles concentration were described in Figure 4. Within the considered Figures 6–8 the particular efforts were devoted to the influence of thermal conductivity ratio and mutual effects of all considered parameters. In the case of $Ra = 10^3$ (Figure 6) a raise of K_r results in a diminution of all considered parameters, while all these parameters decrease with φ also. Significant diminution for $\overline{Nu}$, $|\psi|_{max}$ and θ_{avg} is between $K_r = 1$ and $K_r = 5$, while for $K_r \in (5, 20)$ changes are not so essential. As it has been mentioned above for Figure 4, an increase in φ can decrease θ_{avg} for $Ra = 10^3$.

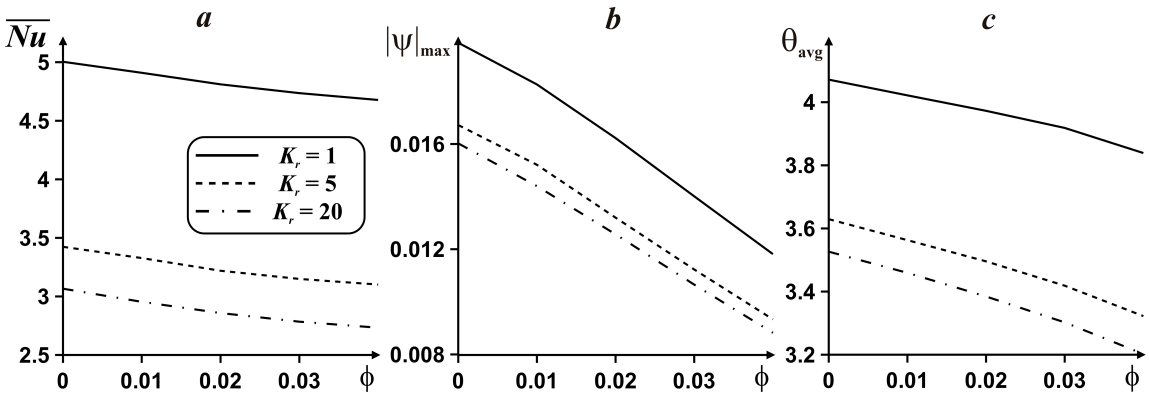

Figure 6. Dependences of the average Nusselt number (**a**), nanoliquid circulation rate (**b**) and mean heater temperature (**c**) on φ and K_r for $Ra = 10^3$, $\delta = 0.2$.

For $Ra = 10^4$ (Figure 7) and $Ra = 10^5$ (Figure 8) the behavior of the considered parameters with K_r is similar to the case of $Ra = 10^3$ (Figure 6), but the main differences are the values of these characteristics. For these Ra, an increment of φ characterizes an enhancement of the heater average temperature that

does not allow to improve the cooling arrangement. Moreover, for high Ra a transition between $K_r = 5$ and $K_r = 20$ becomes insignificant.

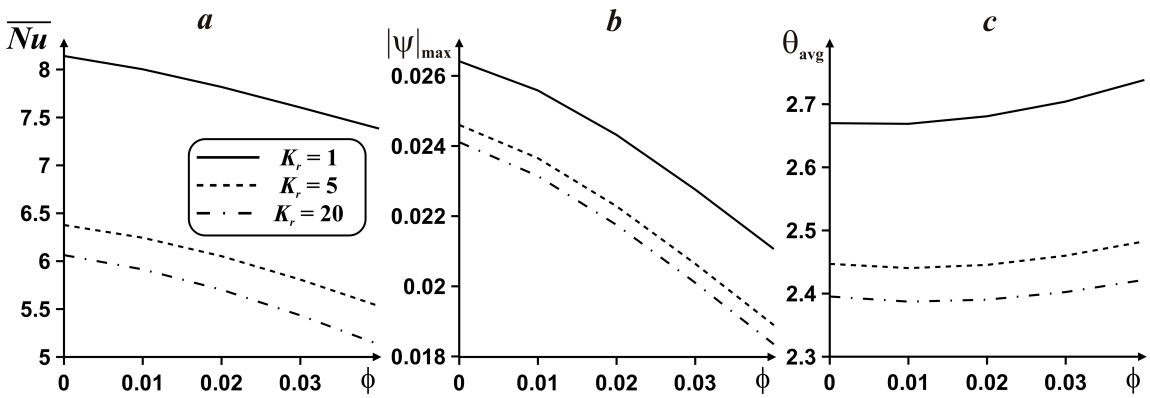

Figure 7. Dependences of the average Nusselt number (**a**), nanoliquid circulation rate (**b**) and mean heater temperature (**c**) on φ and K_r for $Ra = 10^4$, $\delta = 0.2$.

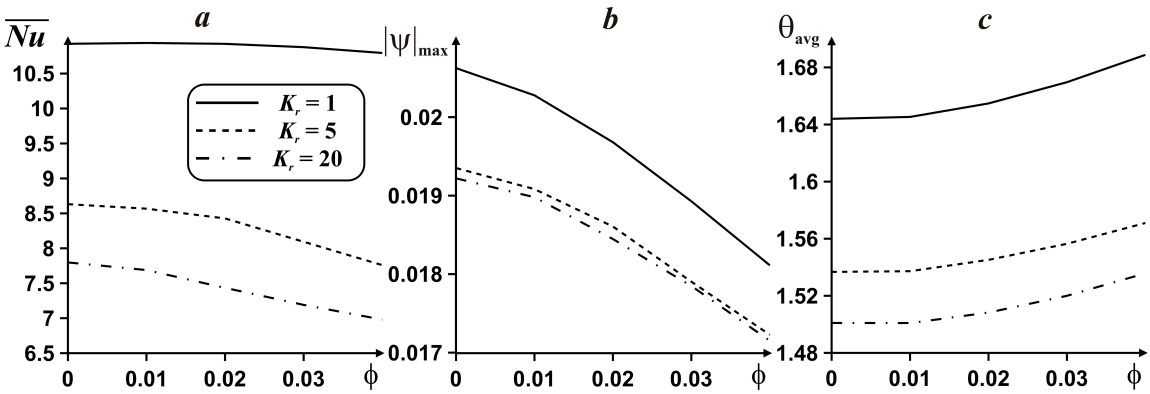

Figure 8. Dependences of the average Nusselt number (**a**), nanoliquid circulation rate (**b**) and mean heater temperature (**c**) on φ and K_r for $Ra = 10^5$, $\delta = 0.2$.

An influence of heater location on isolines of stream function and temperature for $Ra = 10^5$, $K_r = 5$ is demonstrated in Figure 9. A displacement of the heater from the left wall to the right one results in a combination of two recirculations placed in top and bottom part of the domain close to the solid wall and this combined vortex becomes more stable and strong when heater locates near the right vertical border. At the same time, such displacement characterizes a deformation of the penetrative flow from the open port. It is interesting to note that initially for $\delta = 0.1$ (Figure 9a) the power of the upper circulation is high in comparison with the bottom one, while a rise of δ leads to a strengthening of the bottom vortex and an attenuation of the upper one.

For $\delta = 0.3$ (Figure 9c), after a combination of these circulations, we have a convective circulation with two cores and the following increase in δ reflects a growth of the intensity and size of the bottom convective core. Such variations of hydrodynamics are related with modification of temperature field. A presence of penetrative cold flow from the open port characterizes an origin of tilted thermal plume above the heat source. The heating effect of the solid wall from the heater becomes insignificant with an increment of distance between the heat source and solid border. Such feature characterizes a strengthening of the convective circulation appeared near the solid wall. An inclusion of alumina nanoparticles characterizes an origin of combined convective cell near the solid boundary for less value of the length between the heat source and solid border ($\delta = 0.2$) and for $\delta = 0.5$ sizes of this vortex become more powerful in comparison with the case of clear base fluid. Heat conduction effect can be found in the heat-generating element for $\delta = 0.1$ and $\delta = 0.3$ due to more essential interaction between the cooling temperature waves from the solid wall and open port. It is interesting to note

a displacement of the heating zone inside the solid wall from the bottom part (for δ = 0.1) along the vertical coordinate owing to the impact of the tilted thermal plume.

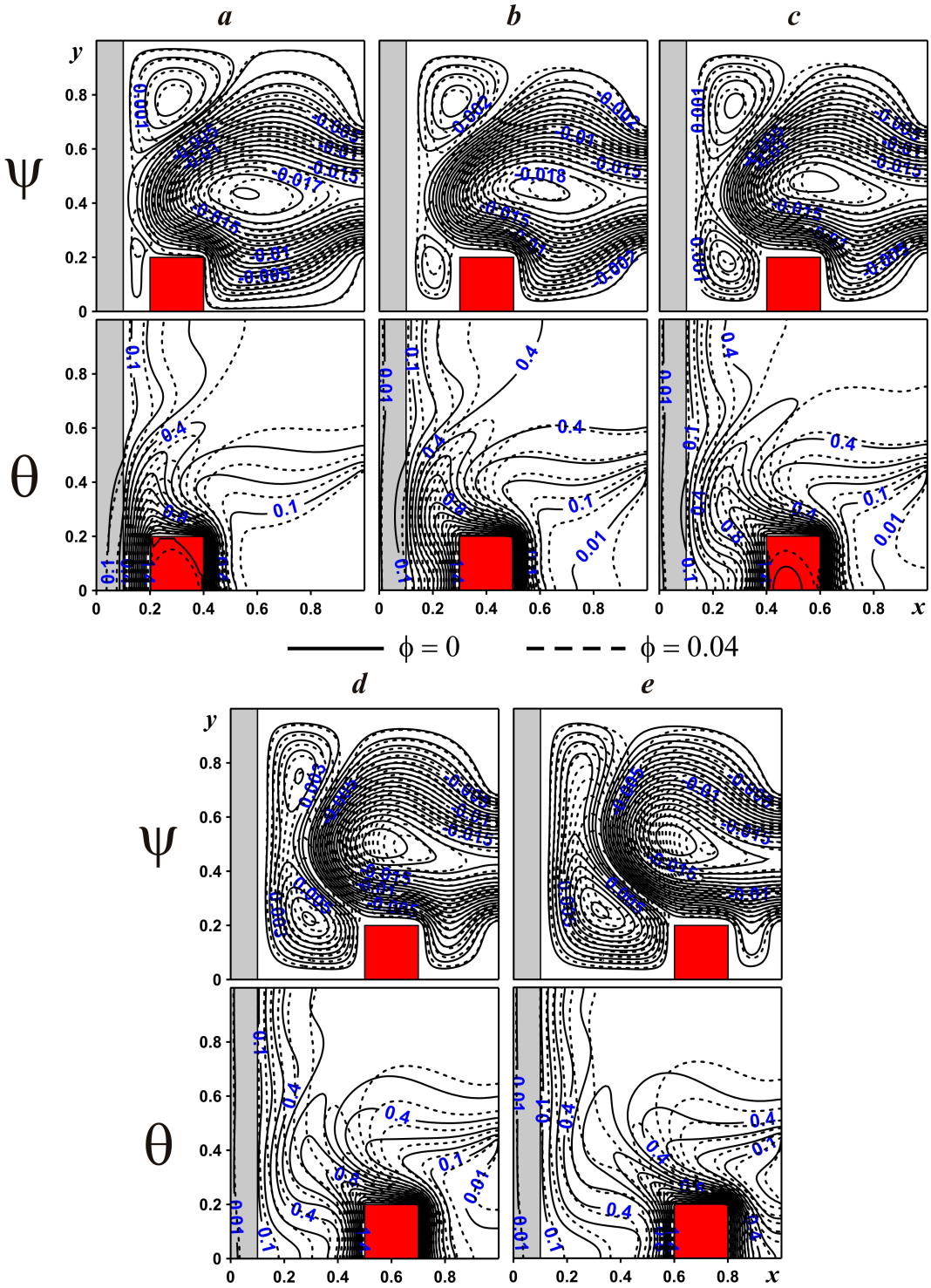

Figure 9. Streamlines ψ and isotherms θ for $Ra = 10^5$, $K_r = 5$: δ = 0.1 (**a**), δ = 0.2 (**b**), δ = 0.3 (**c**), δ = 0.4 (**d**), δ = 0.5 (**e**).

Figures 10–12 illustrate the effects of heater location, thermal conductivity ratio, nanoparticles concentration and Rayleigh number on the average Nusselt number, nanoliquid circulation rate and heater average temperature.

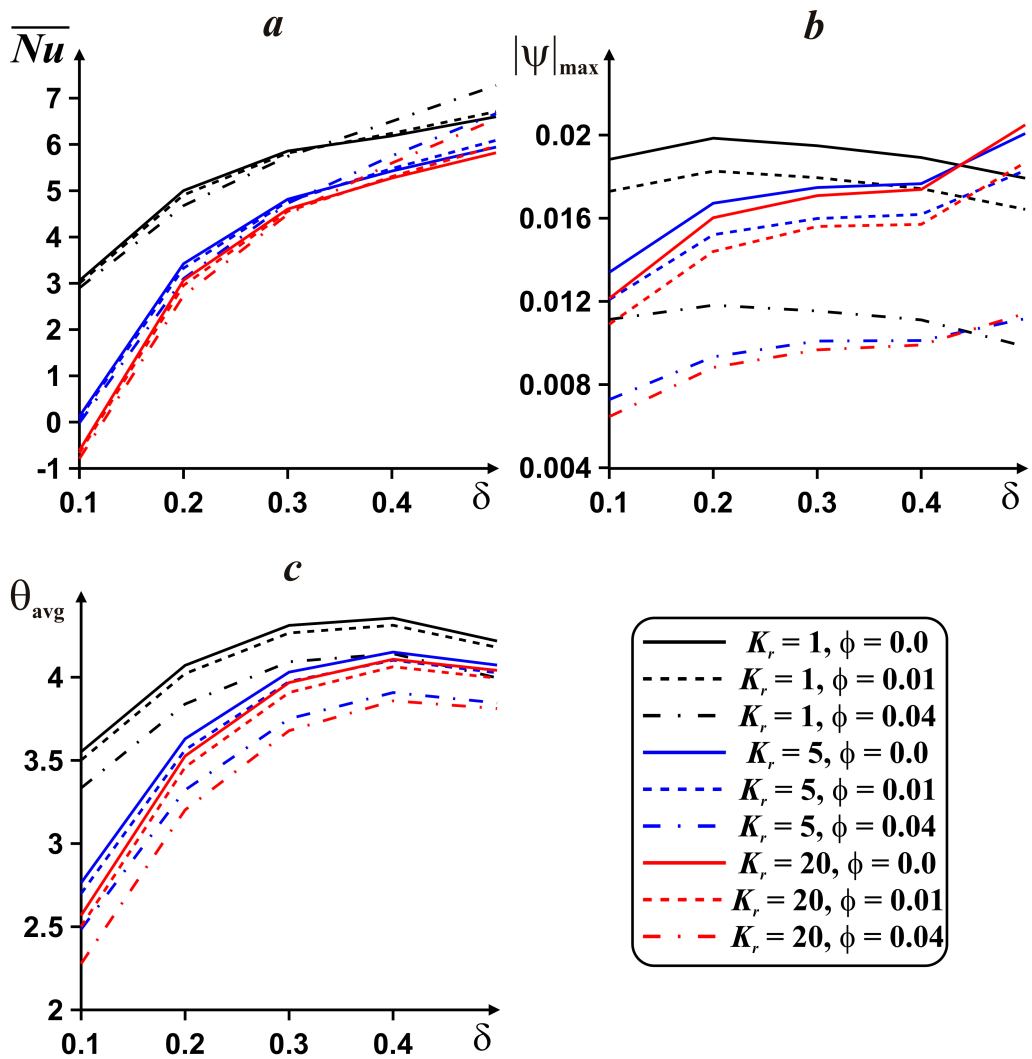

Figure 10. Dependences of the average Nusselt number (**a**), nanoliquid circulation rate (**b**) and mean heater temperature (**c**) on the heater location, thermal conductivity ratio and nanoparticles concentration for $Ra = 10^3$.

In the case of heat conduction dominated regime ($Ra = 10^3$ in Figure 10), a rise of the length between the solid border and heat source results in an increment of $\overline{Nu}$ and this increment is significant for low values of δ, while for $\delta \in (0.3, 0.5)$ the rate of $\overline{Nu}$ is low in comparison with the range of $\delta \in (0.1, 0.3)$. Nanofluid flow rate and heater average temperature have non-monotonic behavior with δ. In the case of $K_r = 1$, a growth of $\delta \in (0.2, 0.5)$ reflects a reduction of $|\psi|_{max}$, while for $K_r = 5$ and $K_r = 20$ $|\psi|_{max}$ increases with δ. The average heater temperature enhances with δ for $\delta \in (0.1, 0.4)$ and for $\delta > 0.4$ it decreases. An enhancement of the thermal conductivity ratio results in a diminution of all considered parameters. The impact of nanoparticles concentration is non-linear for $\overline{Nu}$, namely, $\overline{Nu}$ reduces with φ for $\delta \in (0.1, 0.33)$ and it increases for other values of δ. At the same time, $|\psi|_{max}$ and θ_{avg} are diminished with φ. It is interesting to note the negative values of the average Nusselt number for $K_r = 20$. It means that the temperature gradient along the heater surface is negative due to change of the heat flux direction.

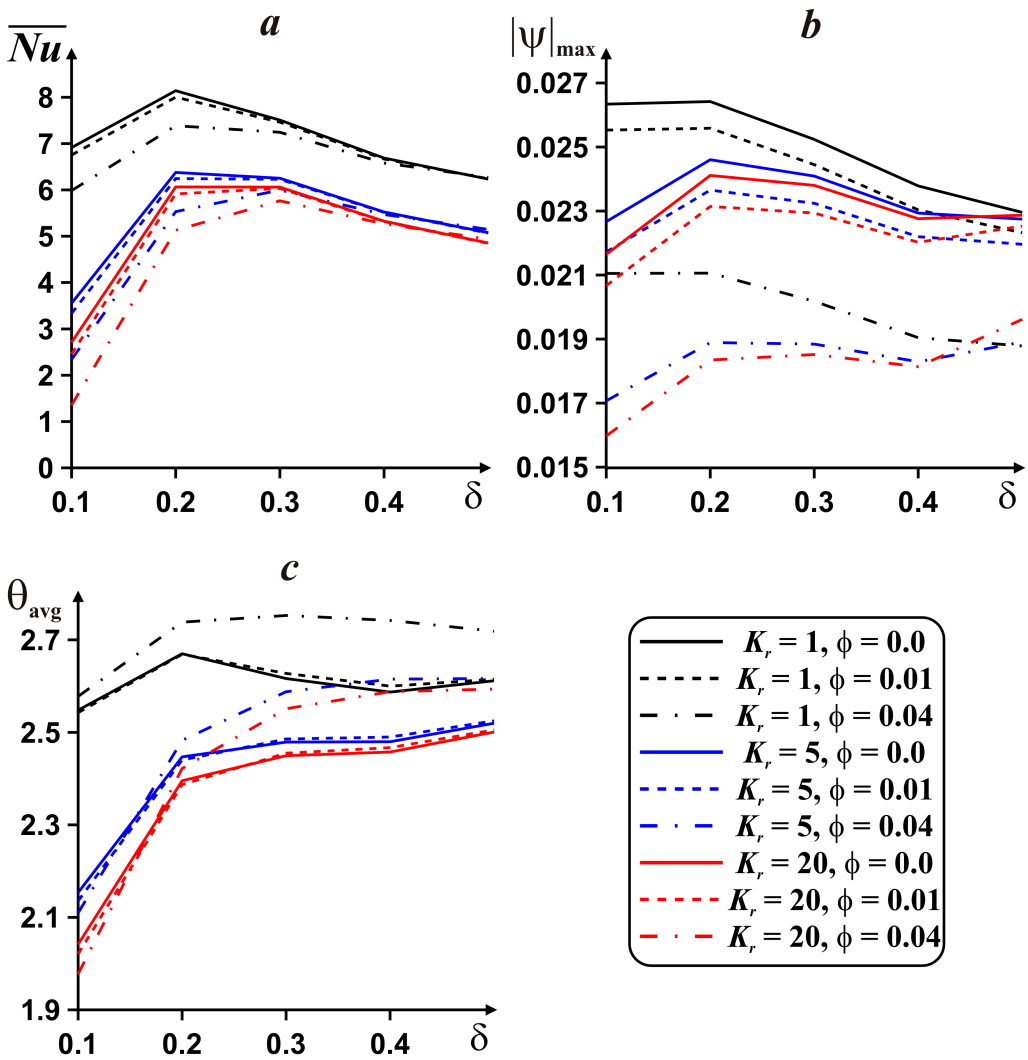

Figure 11. Dependences of the average Nusselt number (**a**), nanoliquid circulation rate (**b**) and mean heater temperature (**c**) on the heater location, K_r and nanoparticles concentration for $Ra = 10^4$.

A non-linear influence of δ on all considered parameters can be found for $Ra = 10^4$ (see Figure 11), namely, for $\delta \in (0.1, 0.2)$ $\overline{Nu}$ and $|\psi|_{max}$ are increased, while for $\delta \in (0.2, 0.5)$ these parameters are reduced. θ_{avg} increases with δ for $K_r = 5$ and $K_r = 20$, while for $K_r = 1$ it has a non-linear behavior. An effect of K_r on the considered parameters is the same like for $Ra = 10^3$ (see Figure 10). $\overline{Nu}$ and $|\psi|_{max}$ are decreased with the nanoparticles volume fraction, while the average heater temperature is changed non-linear with φ.

Behavior of $\overline{Nu}$ with all considered parameters for $Ra = 10^5$ (see Figure 12) is similar to the case of $Ra = 10^4$ (see Figure 11), while the nanoliquid circulation rate and mean heater temperature have the specific behavior.

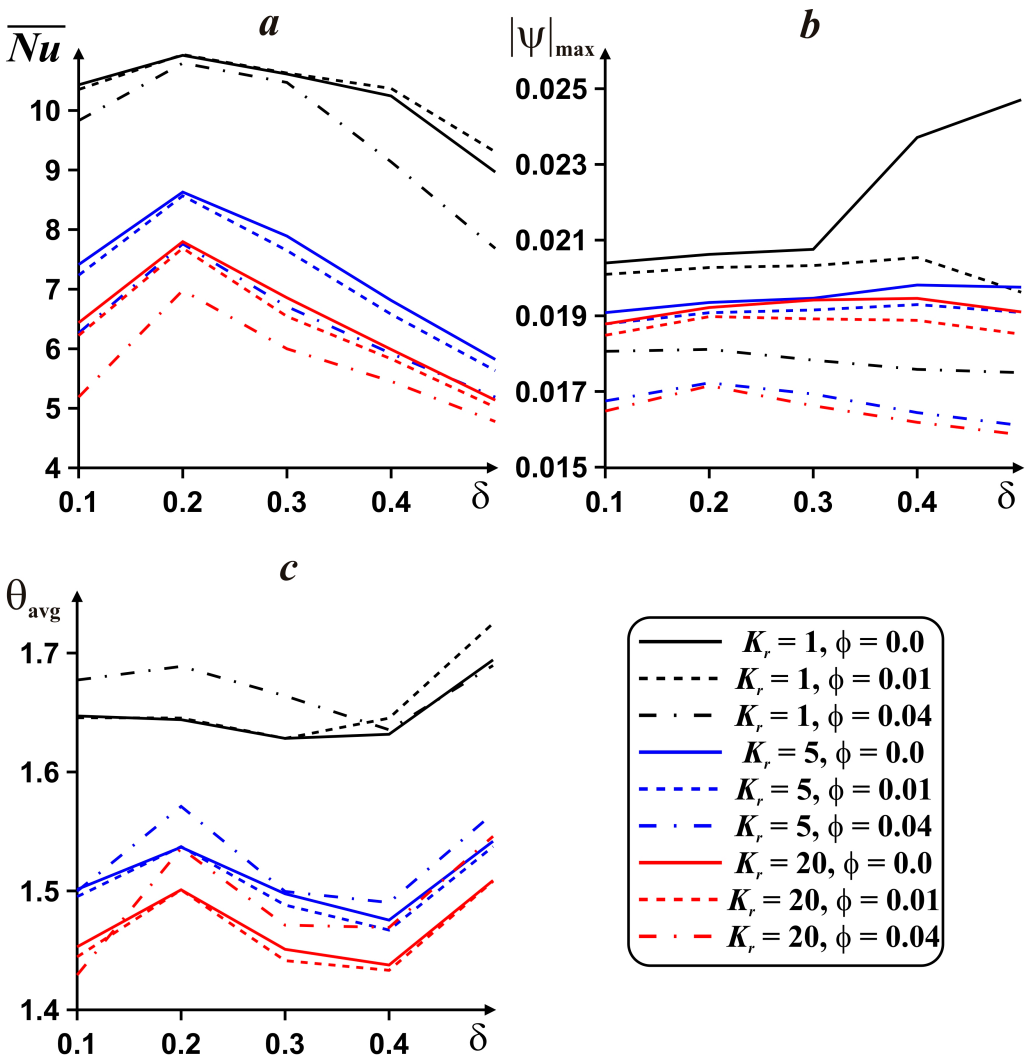

Figure 12. Dependences of the average Nusselt number (**a**), nanoliquid circulation rate (**b**) and mean heater temperature (**c**) on the heater location, K_r and φ for $Ra = 10^5$.

5. Conclusions

Free convection of alumina–water nanoliquid in an open domain with a solid border of finite thickness and heat-generating element has been investigated. Partial differential equations of mathematical physics written using the non-primitive variables have been solved numerically by the finite difference technique. Impacts of Ra, K_r, heater location and nanoparticles volume fraction on liquid circulation and thermal transmission have been investigated. It has been ascertained that an increment of Ra illustrates an enhancement of all considered average characteristics, while a rise of K_r decreases all these parameters. More important parameter for analysis of passive cooling system is an average heater temperature. It is possible to reduce θ_{avg} near the heat-conducting solid wall. A growth of K_r from 1 till 20 for $\varphi = 0$, $\delta = 0.1$ and $Ra = 10^3$ allows to decrease the average heater temperature at 30%, while for $\varphi = 0$, $\delta = 0.1$ and $Ra = 10^4$ average heater temperature decreases at 20% and for $\varphi = 0$, $\delta = 0.1$ and $Ra = 10^5$ θ_{avg} reduces at 12%. An addition of nanosized particles results in a diminution of the average heater temperature near the cooled solid border for all values of Ra and for all heater locations at $Ra = 10^3$. In the case of $\delta = 0.1$, $K_r = 1$ and $Ra = 10^3$ a growth of nanoparticles volume fraction from 0.0 till 0.04 results in a decrease in the average heater temperature at 6%, for $K_r = 5$ the diminution is 10% and for $K_r = 20$ the average heat temperature reduction is 11%. Therefore, alumina-water

nanoparticles and cooling solid wall (thermal conductivity ratio) can be effective characteristics for the passive cooling system of the heat-generating solid element (θ_{avg} can be reduced at 30%).

Author Contributions: M.A.S. and H.F.O. conceived the main concept. M.A.S., H.F.O., and D.V.G. contributed to the investigation and data analysis. M.A.S. and H.F.O. wrote the manuscript. All authors contributed in writing the final manuscript.

Funding: This work of the third author was performed as a government task of the Ministry of Education and Science of the Russian Federation (Project Number 13.7644.2017/BCH). The second and last authors extend their appreciation to the International Scientific Partnership Program ISPP at King Saud University for funding this research work through ISPP#131.

Acknowledgments: Authors thank the respected reviewers for their constructive comments which clearly enhanced the quality of the manuscript.

Conflicts of Interest: The authors declare no conflict of interest.

Abbreviations

The following abbreviations are used in this manuscript:

A	aspect ratio (–)
c	specific heat (J kg^{-1} K^{-1})
d	dimensional open port size (m)
g	gravitational acceleration (m s^{-2})
H	dimensional height of the cavity (m)
h	dimensional distance between the bottom wall and open port (m)
$H_1(\varphi)$, $H_2(\varphi)$, $H_3(\varphi)$, $H_4(\varphi)$, $H_5(\varphi)$	special functions (–)
k	thermal conductivity (W m^{-1} K^{-1})
L	dimensional length of the cavity (m)
l	dimensional thickness of the left solid wall (m)
$\overline{Nu}$	average Nusselt number (–)
p	dimensional pressure (Pa)
Pr	Prandtl number (–)
Q	internal volumetric heat flux (W m^{-3})
Ra	Rayleigh number (–)
s	dimensional distance between the left solid wall and local heater (m)
T	dimensional temperature (K)
t	dimensional time (s)
T_c	ambient nanofluid temperature (K)
u, v	dimensionless velocity components (–)
$\overline{u}$, $\overline{v}$	dimensional velocity components (m s^{-1})
x, y	dimensionless Cartesian coordinates (–)
$\overline{x}$, $\overline{y}$	dimensional Cartesian coordinates (m)
Greek symbols	
α	thermal diffusivity (W m^{-2} K^{-1})
β	thermal expansion coefficient (K^{-1})
ΔT	reference temperature difference (K)
δ	dimensionless distance between the left wall and the heater (–)
ζ	dimensionless distance between the bottom wall and open port (–)
η	dimensionless open port size (–)
θ	dimensionless temperature (–)
μ	dynamic viscosity (kg m^{-1} s^{-1})
ξ	dimensionless thickness of the left solid wall (–)
ρ	density (kg m^{-3})
ρc	heat capacitance (J m^{-3} K^{-1})
$\rho\beta$	buoyancy coefficient (kg m^{-3} K^{-1})
τ	dimensionless time (–)

γ	coordinate along the heater surface (m)
φ	nanoparticles volume fraction (–)
$\overline{\psi}$	dimensional stream function ($m^2\ s^{-1}$)
ψ	dimensionless stream function (–)
$\overline{\omega}$	dimensional vorticity (s^{-1})
ω	dimensionless vorticity (–)
Subscripts	
avg	average
c	cold
f	fluid
hs	heat source
max	maximum value
nf	nanofluid
p	(nano) particle
w	solid wall

References

1. Singh, D.K.; Singh, S.N. Conjugate free convection with surface radiation in open top cavity. *Int. J. Heat Mass Transf.* **2015**, *89*, 444–453. [CrossRef]
2. Mikhailenko, S.A.; Sheremet, M.A.; Mohamad, A.A. Convective-radiative heat transfer in a rotating square cavity with a local heat-generating source. *Int. J. Mech. Sci.* **2018**, *142–143*, 530–540. [CrossRef]
3. Chen, S.; Gong, W.; Yan, Y. Conjugate natural convection heat transfer in an open-ended square cavity partially filled with porous media. *Int. J. Heat Mass Transf.* **2018**, *124*, 368–380. [CrossRef]
4. Naylor, D.; Foroushani, S.S.M.; Zalcman, D. Free convection heat transfer from a window glazing with an insect screen. *Energy Build.* **2017**, *138*, 206–214. [CrossRef]
5. Astanina, M.S.; Sheremet, M.A.; Umavathi, J.C. Transient natural convection with temperature-dependent viscosity in a square partially porous cavity having a heat-generating source. *Numer. Heat Transf. A* **2018**, *73*, 849–862. [CrossRef]
6. Rahman, M.M.; Saidur, R.; Rahim, N.A. Conjugated effect of joule heating and magneto-hydrodynamic on double-diffusive mixed convection in a horizontal channel with an open cavity. *Int. J. Heat Mass Transf.* **2011**, *54*, 3201–3213. [CrossRef]
7. Saha, L.K.; Uddin, K.M.S.; Taher, M.A. Effect of internal heat generation or absorption on MHD mixed convection flow in a lid driven cavity. *Am. J. Appl. Math.* **2015**, *3*, 20–29. [CrossRef]
8. Gangawane, K.M. Effect of angle of applied magnetic field on natural convection in an open ended cavity with partially active walls. *Chem. Eng. Res. Des.* **2017**, *127*, 22–34. [CrossRef]
9. Dong, S.-F.; Li, Y.-T. Conjugate of natural convection and conduction in a complicated enclosure. *Int. J. Heat Mass Transf.* **2004**, *47*, 2233–2239. [CrossRef]
10. Bilgen, E. Natural convection in cavities with a thin fin on the hot wall. *Int. J. Heat Mass Transf.* **2005**, *48*, 3493–3505. [CrossRef]
11. Kristiawan, B.; Santoso, B.; Wijayanta, A.T.; Aziz, M.; Miyazaki, T. Heat transfer enhancement of TiO_2/water nanofluid at laminar and turbulent flows: A numerical approach for evaluating the effect of nanoparticle loadings. *Energies* **2018**, *11*, 1584. [CrossRef]
12. Vryzas, Z.; Kelessidis, V.C. Nano-based drilling fluids: A review. *Energies* **2017**, *10*, 540. [CrossRef]
13. Patil, M.S.; Seo, J.-H.; Kang, S.-J.; Lee, M.-Y. Review on synthesis, thermo-physical property, and heat transfer mechanism of nanofluids. *Energies* **2016**, *9*, 840. [CrossRef]
14. Asirvatham, L.G.; Vishal, N.; Gangatharan, S.K.; Lal, D.M. Experimental study on forced convective heat transfer with low volume fraction of CuO/water nanofluid. *Energies* **2009**, *2*, 97–119. [CrossRef]
15. Raei, B.; Peyghambarzadeh, S.M.; Asl, R.S. Experimental investigation on heat transfer and flow resistance of drag-reducing alumina nanofluid in a fin-and-tube heat exchanger. *Appl. Therm. Eng.* **2018**, *144*, 926–936. [CrossRef]
16. Mehrez, Z.; Bouterra, M.; el Cafsi, A.; Belghith, A. Heat transfer and entropy generation analysis of nanofluids flow in an open cavity. *Comput. Fluids* **2013**, *88*, 363–373. [CrossRef]

17. Sheremet, M.A.; Pop, I.; Ishak, A. Double-diffusive mixed convection in a porous open cavity filled with a nanofluid using Buongiorno's model. *Transp. Porous Media* **2015**, *109*, 131–145. [CrossRef]
18. Sheremet, M.A.; Pop, I.; Shenoy, A. Unsteady free convection in a porous open wavy cavity filled with a nanofluid using Buongiorno's mathematical model. *Int. Commun. Heat Mass Transf.* **2015**, *67*, 66–72. [CrossRef]
19. Bondareva, N.S.; Sheremet, M.A.; Oztop, H.F.; Abu-Hamdeh, N. Heatline visualization of MHD natural convection in an inclined wavy open porous cavity filled with a nanofluid with a local heater. *Int. J. Heat Mass Transf.* **2016**, *99*, 872–881. [CrossRef]
20. Miroshnichenko, I.V.; Sheremet, M.A.; Oztop, H.F.; Abu-Hamdeh, N. Natural convection of Al_2O_3/H_2O nanofluid in an open inclined cavity with a heat-generating element. *Int. J. Heat Mass Transf.* **2018**, *126*, 184–191. [CrossRef]
21. Bondarenko, D.S.; Sheremet, M.A.; Oztop, H.F.; Ali, M.E. Natural convection of Al_2O_3/H_2O nanofluid in a cavity with a heat-generating element. Heatline visualization. *Int. J. Heat Mass Transf.* **2019**, *130*, 564–574. [CrossRef]
22. Ho, C.J.; Liu, W.K.; Chang, Y.S.; Lin, C.C. Natural convection heat transfer of alumina-water nanofluid in vertical square enclosures: An experimental study. *Int. J. Therm. Sci.* **2010**, *49*, 1345–1353. [CrossRef]
23. Saghir, M.Z.; Ahadi, A.; Mohamad, A.; Srinivasan, S. Water aluminum oxide nanofluid benchmark model. *Int. J. Therm. Sci.* **2016**, *109*, 148–158. [CrossRef]
24. Mohamad, A.A.; El-Ganaoui, M.; Bennacer, R. Lattice Boltzmann simulation of natural convection in an open ended enclosure. *Int. J. Therm. Sci.* **2009**, *48*, 1870–1875. [CrossRef]
25. Kefayati, G.H.R. Effect of a magnetic field on natural convection in an open cavity subjugated to water/alumina nanofluid using Latttice Boltzmann Method. *Int. Commun. Heat Mass Transf.* **2013**, *40*, 67–77. [CrossRef]